Original Article

The m^{6}A demethylase fat mass and obesity-associated protein mitigates pyroptosis and inflammation in doxorubicin-induced heart failure via the toll-like receptor 4/NF-κB pathway

Weiling Tu, Xiao Huang, Songtao Liu, Yuliang Zhan, Xinyong Cai, Liang Shao^

Department of Cardiology, Jiangxi Provincial People's Hospital, the First Affiliated Hospital of Nanchang Medical College, Nanchang, China

Contributions: (I) Conception and design: W Tu, X Huang, S Liu; (II) Administrative support: L Shao; (III) Provision of study materials or patients: W Tu, X Huang, S Liu, Y Zhan, X Cai; (IV) Collection and assembly of data: W Tu, X Huang, S Liu, Y Zhan, X Cai; (V) Data analysis and interpretation: W Tu, X Huang, S Liu; (VI) Manuscript writing: All authors; (VII) Final approval of manuscript: All authors.

Correspondence to: Liang Shao, MD. Department of Cardiology, Jiangxi Provincial People's Hospital, the First Affiliated Hospital of Nanchang Medical College, No. 152, Aiguo Road, Nanchang 330006, China. Email: shaoliang5201@126.com.

Background: Doxorubicin (Dox) can induce cardiotoxicity, thereby restricting the utility of this potent drug. Herein, the study ascertained the mechanism of the N6-methyladenosine (m^{6}A) demethylase fat mass and obesity-associated protein (FTO) in pyroptosis and inflammation during Dox-induced heart failure (HF).

Methods: Serum samples were collected from HF patients for detection of the expression of FTO and toll-like receptor 4 (TLR4). Dox-treated H9C2 cardiomyocytes were chosen for *in vitro* HF modeling, followed by measurement of FTO and TLR4 expression. Cardiomyocytes were detected for viability, apoptosis, spatial distribution of NOD-, LRR- and pyrin domain-containing protein 3 (NLRP3), and the levels of lactic dehydrogenase, inflammatory factors, oxidative stress markers, and pyroptosis-related proteins. The m^{6}A levels of mRNA were examined. RNA immunoprecipitation (RIP) and mRNA stability measurement were used to determine mRNA and protein expression, and RNA m^{6}A dot blot and methylated-RIP assay were performed to detect m^{6}A methylation levels. The expression of p-NF-κB p65 and p-IκB-α was measured by western blotting.

Results: In the serum of HF patients, FTO was elevated while TLR4 was decreased. Dox treatment reduced FTO expression and increased m^{6}A methylation levels and TLR4 expression in H9C2 cells. Overexpression of FTO and knockdown of TLR4 reduced apoptosis, cytotoxicity, inflammation, pyroptosis, oxidative stress, NLRP3 co-localization, and fluorescence intensity in Dox-induced H9C2 cells. Mechanistically, FTO resulted in reduced binding activity of YTHDF1 to TLR4 mRNA via m^{6}A demethylation of TLR4, thus declining TLR4, p-NF-κB p65, and p-IκB-α expression. TLR4 knockdown counteracted the effects of FTO knockdown on Dox-induced H9C2 cells.

Conclusions: FTO alleviated Dox-induced HF by blocking the TLR4/NF-κB pathway.

Keywords: Doxorubicin (Dox); heart failure (HF); fat mass and obesity-associated protein (FTO); toll-like receptor 4 (TLR4); N6-methyladenosine modification (m^{6}A modification)

Submitted Aug 01, 2023. Accepted for publication Nov 17, 2023. Published online Jan 30, 2024.
doi: 10.21037/cdt-23-326
View this article at: https://dx.doi.org/10.21037/cdt-23-326

^ ORCID: 0000-0003-3092-6229.

Introduction

Doxorubicin (Dox) is a type of effective chemotherapeutic drug for cancer treatment (1). Unfortunately, Dox has undesirable cardiotoxic effects, which restricts the use of this potent drug (2). Reportedly, Dox-based chemotherapy can cause the occurrence of cardiomyopathy and heart failure (HF) (3,4), as well as morbidity and mortality (5). Apoptosis is the most frequent last stage leading to cardiomyocyte death in Dox-induced cardiotoxicity, and oxidative stress and inflammation are critical factors implicated in Dox-induced cardiomyocyte apoptosis (6). In addition to apoptosis, long-term Dox-based chemotherapy results in multiple kinds of cardiomyocyte death, including ferroptosis and pyroptosis, to cause cardiotoxicity (7). Pyroptosis is a type of pro-inflammatory programmed cell death that has garnered growing attention due to its association with innate immunity and diseases (8). Importantly, pyroptosis has been demonstrated to participate in the development of Dox-induced HF (9). Accordingly, for the sake of understanding the pathogenesis of Dox-induced HF, it is important to discuss molecular mechanisms underlying cardiomyocyte pyroptosis, oxidative stress, and inflammation.

As the most frequent internal modification in mRNAs, N6-methyladenosine (m^6A) influences stability, translation, and processing of RNA (10). Fat mass and obesity-associated protein (FTO) is the first discovered RNA m^6A demethylase, which is dysregulated and plays an essential role in many cancers (11). A prior study revealed that FTO downregulation and elevated m^6A modification was involved in decreased cardiac contraction during HF (12). Moreover, another study reported that FTO bound to toll-like receptor 4 (TLR4) mRNA to contribute to the loss of m^6A sites in TLR4 mRNA in the ipsilateral thalamus (13). TLR4 is vital for innate immunity, whose hyperactivation produces numerous inflammatory factors, contributing to the development of many diseases, including acute lung injury and cardiovascular diseases (14). Dox can enhance TLR4 expression and NOD-, LRR- and pyrin domain-containing protein 3 (NLRP3) inflammasome formation to initiate pyroptosis in H9C2 cells (15). TLR4 downregulation is involved in the cardioprotective role of CTRP5 in Dox-induced cardiotoxicity by impeding oxidative stress and inflammation (16). The downstream gene of TLR4, which controls the expression of inflammatory factors, is nuclear factor kappa B (NF-B) (17). Moreover, baicalein mediates the TLR4/inhibitory protein κB (IκB)-α/NF-κB pathway to prevent inflammation and ultimately curb Dox-induced cardiotoxicity (18). YT521-B homology domain-containing protein 1 (YTHDF1), as a reader protein of m^6A, has been reported to regulate mRNA degradation and increase translation efficiency (19). Methyltransferase-like 14, YTHDF1, and FTO regulate SOCS1 m^6A methylation and maintain appropriate Socs1 levels, thereby maintaining a negative feedback loop of lipopolysaccharide/TLR4/NF-κB signaling that controls inflammation in macrophages (20).

In this context, we reasonably hypothesized that FTO might modulate the TLR4/NF-κB pathway via YTHDF1, thereby regulating the onset of Dox-induced HF. Herein, our study probed whether FTO manipulated cardiomyocyte pyroptosis, oxidative stress, and inflammation in Dox-induced HF by affecting the m^6A modification of TLR4 and then the TLR4/NF-κB pathway.

Highlight box

Key findings

- In this study, we found that N6-methyladenosine (m^6A) demethylase fat mass and obesity-associated protein (FTO) is involved in pyroptosis and inflammation in heart failure (HF) via the toll-like receptor 4 (TLR4)/nuclear factor kappa B (NF-κB) axis.

What is known and what is new?

- It is known that the TLR4/NF-κB axis not only activates the secretion of inflammatory cytokines, but also promotes the NOD-, LRR- and pyrin domain-containing protein 3 inflammasome mediated pyroptosis of cells.
- On this basis, we found that FTO was involved in mRNA demethylation to regulate the expression of TLR4 and then affected the TLR4/NF-κB signaling pathway.

What is implication and what should change now?

- Our findings provide novel insights for further understanding of the mechanism of m^6A methylation in HF.

Methods

Serum sample collection

This study recruited 20 patients diagnosed with chronic HF in Jiangxi Provincial People's Hospital, all of whom met the "Guidelines for Diagnosis and Treatment of Heart Failure in China 2014". The guidelines define HF as a complex group of clinical syndromes in which ventricular filling or ejection ability is impaired due to any structural or functional abnormality of the heart. The main clinical manifestations are dyspnea and fatigue (limited activity tolerance), and fluid retention (pulmonary congestion

and peripheral edema). HF is a serious and terminal stage of various heart diseases, with a high incidence and is one of the most important cardiovascular diseases today. During the same period, the control group consisted of 20 healthy individuals who came to Jiangxi Provincial People's Hospital for physical examination. All patients or their families provided informed consent for the study. The study was approved by the Medical Ethics Committee of Jiangxi Provincial People's Hospital (No. 2022120210) and adhered to the Declaration of Helsinki (as revised in 2013).

Each study subject's 4 mL of fasting venous blood was collected in the morning and centrifuged at 1,000 g for 10 min. The supernatant was then placed into a clean eppendorf (EP) tube, labeled, and frozen at –20 ℃. Then, the expression levels of FTO and TLR4 in the supernatant was measured through reverse transcription quantitative polymerase chain reaction (RT-qPCR).

Cell culture, treatment, and transfection

H9C2 cells (rat cardiomyocyte cell line; CBP60588, Cobioer Biosciences Co., Ltd., Nanjing, China) were cultured in Dulbecco's Modified Eagle Medium (E600003, Sangon, Shanghai, China) with 10% fetal bovine serum (E600001, Sangon) and 1% penicillin and streptomycin (Sangon) under the conditions of 37 ℃, 95% O_2, and 5% CO_2. The medium was renewed every other day.

H9C2 cells were randomly grouped: control [cells were treated with dimethyl sulfoxide (DMSO)], various concentrations of Dox [treated with different concentrations (0.5, 1, 1.5, 2 μM) of Dox (SC0159, Beyotime, Shanghai, China) diluted by DMSO to simulate Dox damage *in vitro*], overexpression (oe)-negative control (NC), oe-FTO, small interfering (si)-NC, si-FTO, si-NC, si-TLR4, si-NC + si-NC, si-FTO + si-NC, and si-FTO + si-TLR4 groups. The extent of damage to H9C2 cells by different concentrations of Dox was determined by detecting cell viability, and the most damage-sensitive concentration was selected for subsequent cell experiments.

FTO overexpression vectors (oe-FTO) and empty vector plasmids (oe-NC) were generated using pcDNA3.1 plasmids. Small interfering RNAs of FTO (si-FTO) and TLR4 (si-TLR4) and their NC (si-NC) were generated with siRNA plasmids purchased from Ribobio (Guangzhou, China). Cells were transfected with these vectors at a dose of 2 μg as instructed in the manuals of Lipofectamine™ 2000 for 4 h, and the transfected cells were cultured in normal medium for 24 h. Next, cells were exposed to an optimal concentration of Dox for 24 h *in vitro* Dox damage for subsequent cell. The used siRNA sequences were as follows: si-FTO, GGATGACTCTCATCTCGAA; si-TLR4, GCGUACAGGUUGUUCCUAA; si-NC, UUCUCCGAACGUGUCACGU.

Cell counting kit-8 (CCK-8) assay

Subsequent to 24-h treatment of H9C2 cells with different concentrations of Dox, cell viability was measured with a CCK-8 kit (C0037, Beyotime). Optical density (OD) values at 450 nm were measured with a microplate reader (SpectraMax 190, Molecular Device, Sunnyvale, CA, USA).

Flow cytometry

H9C2 cell apoptosis was assessed by flow cytometry with an Annexin V-fluorescein isothiocyanate (FITC)/propidium iodide (PI) double staining kit (KGA105, KeyGEN, Nanjing, China). Annexin V-FITC and PI were used to analyze phosphatidylserine outside the membrane of apoptotic cells to identify apoptotic and necrotic cells. Cells were briefly collected using trypsin and subjected to three washes with phosphate-buffered saline (PBS). Thereafter, cells were then resuspended in 500 μL of 4-(2-hydroxyethyl)-1-piperazineethanesulfonic acid buffer (C0215, Beyotime), followed by 5-min culture with 5 μL of Annexin V-FITC and 5 μL of PI at room temperature in the dark and analysis on a flow cytometer (BD Biosciences, Franklin Lakes, NJ, USA).

Lactic dehydrogenase (LDH) assay

The cytotoxicity of total cells was evaluated by measuring the release of LDH from the cells. Following Dox treatment of H9C2 cells, the medium was obtained for measuring LDH activity in the cell supernatant on a biochemical autoanalyzer (LABOSPECT 008 AS, Hitachi, Kokubunji, Japan).

Enzyme-linked immunosorbent assay (ELISA)

The levels of interleukin (IL)-1β, IL-6, IL-18, and tumor necrosis factor alpha (TNF-α) in H9C2 cells were tested as per the protocols of commercially available ELISA kits (PI303, PI328, PI555, and PT516; Beyotime).

Detection of oxidative stress markers

H9C2 cardiomyocytes were obtained for analyzing

Table 1 The primers used for RT-qPCR

Genes	Sequences
Human FTO	F: 5'-CGAGAGCGCGAAGCTAAGA-3'
	R: 5'-GCTGCCACTGCTGATAGAAT-3'
Rat FTO	F: 5'-TGAAGGTAGCGTGGGACATAGA-3'
	R: 5'-GGTGAAAAGCCAGCCAGAAC-3'
Human TLR4	F: 5'-TCCCTGCATAGAGGTAGTTCC-3'
	R: 5'-AGAGGTGGTGTAAGCCATGC-3'
Rat TLR4	F: 5'-TGCGGGTTCTACATCAAA-3'
	R: 5'-CCATCCGAAATTATAAGAAAAGTC-3'
YTHDF1	F: 5'-ACAGTTACCCCTCGATGAGTG-3'
	R: 5'-GGTAGTGAGATACGGGATGGGA-3'
YTHDF2	F: 5'-GAGCAGAGACCAAAAGGTCAAG-3'
	R: 5'-CTGTGGGCTCAAGTAAGGTTC-3'
YTHDF3	F: 5'-GATCAGCCTATGCCATATCTGAC-3'
	R: 5'-CCCCTGGTTGACTAAAAACACC-3'
GAPDH	F: 5'-GCACCGTCAAGGCTGAGAAC-3'
	R: 5'-TGGTGAAGACGCCAGTGGA-3'

RT-qPCR, reverse transcription quantitative polymerase chain reaction; FTO, fat mass and obesity-associated protein; TLR4, toll-like receptor 4; GAPDH, glyceraldehyde-3-phosphate dehydrogenase; F, forward; R, reverse.

myocardial oxidative stress. Malondialdehyde (MDA) and superoxide dismutase (SOD) activities were measured in accordance with the protocols of ELISA kits (S0131S and S0101S; Beyotime).

Immunofluorescence staining

Following three PBS washes, the treated H9C2 cells were fixed in 4% paraformaldehyde for 30 min, permeabilized with 0.5% Triton X-100 for another 30 min, and subsequently cultured with immunofluorescence staining blocking solution (P0102, Beyotime) to prevent non-specific protein interactions. Next, cells underwent overnight incubation with primary NLRP3 antibody (1:200, DF7438, Affinity, Jiangsu, China) at 4 ℃, followed by 2 h of co-incubation with the secondary antibody goat anti-rabbit immunoglobulin G IgG H&L Fluor488 (1:100, S0018, Affinity). Fluorescence images were captured with a fluorescence microscopy system (IX5, Olympus, Tokyo, Japan).

RT-qPCR

Total RNA of cardiomyocytes was extracted and reversely transcribed to cDNA with the PrimeScript One-step RT-PCR kit (Takara, Tokyo, Japan). The used primers were designed and synthesized by Takara (*Table 1*). RT-qPCR was carried out with a LightCycler 480 SYBR Green Master (04707516001, Roche, Basel, Switzerland) under the following reaction conditions: pre-denaturation at 95 ℃ for 10 min and 40 cycles of denaturation at 95 ℃ for 10 s, annealing at 60 ℃ for 20 s, and extension at 72 ℃ for 34 s. The relative transcript level of the target gene was determined using the relative quantification method ($2^{-\Delta\Delta CT}$), with glyceraldehyde-3-phosphate dehydrogenase (GAPDH) as the normalizer.

Western blotting

Total protein was extracted from frozen cell lysates using Radio-Immunoprecipitation Assay reagents (P0013B, Beyotime). The supernatant was obtained after 30-min incubation on ice at 4 ℃ and 10-min centrifugation at 8,000 g. The total protein concentration was measured with a bicinchoninic acid kit. Thereafter, 50 μg of protein was dissolved in 2× sodium dodecyl sulfate (SDS) loading buffer and subjected to 5 min of boiling at 100 ℃. Following separation by 10% SDS-polyacrylamide gel electrophoresis, the protein was transferred to a polyvinylidene fluoride membrane (FFP19, Beyotime). The membrane then underwent sealing with 5% skim milk at room temperature and overnight incubation with primary antibodies against FTO (1:1,000, ab280081, Abcam, Cambridge, UK), TLR4 (1:1,000, ab217274, Abcam), phosphorylation (p)-NF-κB p65 (1:200, sc-136548, Santa Cruz Biotechnology, Santa Cruz, CA, USA), p-IκB-α (1:200, sc-8404, Santa Cruz Biotechnology), NLRP3 (1:1,000, ab263899, Abcam), apoptosis-associated speck-like protein containing a CARD (ASC; 1:1,000, DF6304, Affinity), Cleaved Caspase-1 (1:800, AF4022, Affinity), gasdermin D N-terminal domain (GSDMD-N; 1:2,000, DF13758, Affinity), and GAPDH (1:500, ab8245, Abcam; the normalizer) at 4 ℃. The membrane was rinsed with Tris-buffered saline containing Tween 20 and placed on clean glass plates after 1h of incubation with secondary goat anti-rabbit IgG H&L [horseradish peroxidase (HRP)] antibody (1:2,000, ab6702, Abcam) at 37 ℃. The membrane was scanned with an Odyssey infrared imaging system (LI-COR Biosciences, Lincoln, NE, USA) and then analyzed with the Quantity One v4.6.2 software.

Quantification of m^{6}A modifications

Following treatment with DNase I reagents (D7073, Beyotime), total RNA isolation was isolated using TRIzol reagents (15596018, Invitrogen, Carlsbad, CA, USA) in accordance with the manufacturer's instructions. RNA quality was analyzed with NanoDrop. Changes in all m^{6}A levels in mRNA were measured as per the protocols of the EpiQuik m^{6}A RNA Methylation Quantification Kit (P-9005-48, Epigentek, Farmingdale, NY, USA). Poly-A-purified RNA (200 ng) was employed for analyzing each sample. In summary, 200 ng of RNA was coated on the assay wells. Subsequently, the captured antibody solution and detection antibody solution were then added to the assay wells at an appropriate dilution concentration. m^{6}A levels were quantified with colorimetry by reading the absorbance at 450 nm, followed by calculation based on the standard curve.

RNA immunoprecipitation (RIP) assay

The RIP assay was performed as per the manuals of the Magna RIP RNA Binding Protein Immunoprecipitation Kit (Millipore, Billerica, MA, USA). In detail, the cells were submerged in the RIP lysis buffer and reacted with antibodies against FTO [1:50, #31687, Cell Signaling Technologies (CST), Beverly, MA, USA], YTH N6-methyladenosine RNA binding protein 1 (YTHDF1; 1:50, #57530, CST), YTHDF2 (1:100, #71283, CST), YTHDF3 (1:100, #24206, CST), or rabbit IgG (1:100, ab172730, Abcam) overnight at 4 ℃, followed by washing with RIP washing buffer at 4 ℃ for 10 min and then with RIP lysis buffer at 4 ℃ for 5 min. The co-precipitated RNA was purified with phenol: chloroform: isoamyl alcohol and subjected to qPCR.

mRNA stability measurement

H9C2 cells after FTO or YTHDF1 knockdown were treated with 1 μg/mL actinomycin D (A937, Sigma-Aldrich, St. Louis, MO, USA). Samples were harvested at 0, 3, and 6 h for total RNA extraction and cDNA synthesis, which were performed according to the method described above (21). Finally, qPCR was conducted to quantify mRNA levels.

RNA m^{6}A dot blot

The RNA was denatured at 65 ℃ for 5 min before cooling on ice for the m^{6}A dot blot. After being double diluted, the 5 L of RNA (800 ng) was spotted on the Amersham Hybond N+ membrane (GE Healthcare, Piscataway, NJ, USA). The membrane was exposed to ultraviolet light three times before being washed with PBS, sealed with nucleic acid blocking buffer (89880A, Thermo Fisher Scientific, Waltham, MA, USA) for 1 h, and then incubated overnight at 4 ℃ with anti-m^{6}A antibody (1:1,000, ab151230, Abcam). After the incubation of the membrane with HRP-coupled anti-rabbit IgG secondary antibody (1:500, Invitrogen), staining was displayed with the diaminobenzidine peroxidase substrate kit (P0202, Beyotime).

Methylated-RNA immunoprecipitation (Me-RIP) assay

MeRIP assay was performed with a reported protocol (22). Briefly, mRNA was first purified from total RNA with the PolyATtract mRNA Isolation System (Z5210, Promega, Madison, WI, USA). One-tenth of the mRNA was stored as Input. Magnetic beads were incubated with anti-m^{6}A antibody (ab286164, Abcam) or IgG antibody for 4 h at 4 ℃. After three washes, the magnetic beads were mixed with RIP buffer and fragmented RNA for overnight incubation at 4 ℃. Following Proteinase K digestion, the methylated mRNAs were purified with ethanol and subjected to qPCR for detecting the abundance of TLR4 mRNA.

Statistical analysis

Statistical analysis was performed with GraphPad Prism 8 software (GraphPad Software Inc., San Diego, CA, USA). Data were presented as mean ± standard deviation or number. With Tukey's multiple comparisons test as the *post hoc* analysis, differences were examined within groups using the unpaired *t*-test and across multiple groups using one-way analysis of variance. In all statistical analyses, a P value <0.05 was considered statistically significant.

Results

Reduced FTO and elevated TLR4 levels in serum of HF patients

To verify the expression levels of FTO and TLR4 in HF patients, we first recruited 20 patients with chronic HF and 20 healthy individuals. HF was significantly correlated with left ventricular ejection fraction and Dox use, with statistically significant differences, according to the clinicopathologic characteristics of the patients and healthy controls, but it was unrelated to age, sex, body mass index,

Table 2 Clinicopathologic feature

Clinical features	Healthy individuals (n=20)	HF patients (n=20)	Statistical value	P value
Age (years)	51.12±6.69	53.27±7.03	t=0.991	0.328
Sex			χ^2=0.960	0.327
Male	14	11		
Female	6	9		
BMI (kg/m^2)	24.27±2.29	24.11±1.84	t=0.207	0.837
Smoking			χ^2=0.440	0.507
Yes	6	8		
No	14	12		
Alcohol consumption			χ^2=1.616	0.204
Yes	9	13		
No	11	7		
Dox			χ^2=17.14	<0.0001*
Yes	0	12		
No	20	8		
LVEF (%)	63.21±6.14	38.54±4.16	t=14.88	<0.0001*

Data were presented as mean ± standard deviation or number, followed by Chi-squared test and Student t-test. *, P<0.05, and the difference is statistically significant. HF, heart failure; BMI, body mass index; Dox, doxorubicin; LVEF, left ventricular ejection fraction.

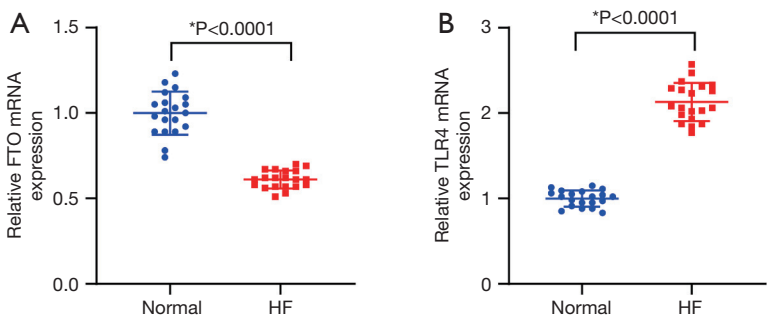

Figure 1 Low expression of FTO and high expression of TLR4 in HF patients. (A) RT-qPCR to detect the expression level of FTO in HF patients. (B) RT-qPCR to detect the expression level of TLR4 in HF patients. N=20, the data are expressed in mean ± standard deviation. Unpaired t-test was adopted for the comparison of two groups of data with normal distribution, and Tukey's test for *post hoc* test. *, compared with the normal group, P<0.05. HF, heart failure; FTO, fat mass and obesity-associated protein; TLR4, toll-like receptor 4; RT-qPCR, reverse transcription quantitative polymerase chain reaction.

smoking, and alcohol consumption, with no statistically significant differences (*Table 2*). Their blood samples were collected and centrifuged to separate the serum for detection of the levels of FTO and TLR4 through RT-qPCR. Compared with healthy volunteers, the serum FTO content of HF patients was reduced, while TLR4 was significantly increased (*Figure 1A,1B*).

FTO is lowly expressed in the cardiomyocyte model of HF, and FTO inhibits Dox-induced cardiomyocyte pyroptosis, inflammation, and oxidative stress

To measure FTO expression in HF, H9C2 cardiomyocytes were first treated with different concentrations of Dox (0.5, 1, 1.5, and 2 μM) to establish an HF cell model, followed

by determination of the optimal concentration of Dox for further experiments. The cell viability assay results (*Figure 2A*) revealed that H9C2 cardiomyocyte viability was lowest at a Dox concentration of 1 μM. Accordingly, subsequent cell experiments were performed at this concentration. Next, FTO expression was measured in Dox (1 μM)-treated H9C2 cells. This revealed that FTO expression was significantly lower in Dox-treated H9C2 cardiomyocytes than in control H9C2 cells (*Figure 2B*).

In addition, overexpression vectors and specific siRNA of FTO were designed to probe the biological effects of FTO on HF. RT-qPCR and western blotting (*Figure 2C*) demonstrated that FTO expression in H9C2 cells increased after oe-FTO transfection but decreased markedly in response to si-FTO transfection. After the transfection efficiency was determined, the effect of FTO on HF was analyzed at the cellular function level. Flow cytometry and cytotoxicity assay demonstrated that FTO upregulation substantially reduced apoptosis (*Figure 2D*) and LDH production (*Figure 2E*) in Dox-treated H9C2 cells, whereas FTO knockdown significantly increased both. FTO hypothesized that some relevant cytokines are important in HF after analyzing the above results. In this regard, the levels of inflammatory factors (IL-18, IL-1β, TNF-α, and IL-6) and oxidative stress factors (MDA and SOD) in cells were tested. The results (*Figure 2F,2G*) manifested that FTO overexpression diminished the levels of inflammatory factors and MDA but elevated SOD levels in Dox-treated H9C2 cells, while FTO knockdown caused opposite trends. The expression of pyroptosis-related proteins (NLRP3, ASC, Cleaved Caspase-1, and GSDMD-N) was then examined using western blotting to determine the effect of FTO on cardiomyocytes via pyroptosis. The results (*Figure 2H*) presented that the expression of pyroptosis proteins was reduced by FTO overexpression but augmented subsequent to FTO knockdown. NLRP3 immunofluorescence staining (*Figure 2I*) also exhibited that FTO blocked the assembly of NLRP3 inflammasomes, characterized by less NLRP3 co-localization and lower fluorescence intensity. Furthermore, the fluorescence intensity of NLRP3 in Dox-treated cardiomyocytes was considerably elevated, which indicated that upregulation of FTO may inhibit the progression of caspase-1-dependent inflammatory apoptosis by inhibiting NLRP3 inflammasome activation.

In summary, FTO expression was low in the cell model of Dox-induced HF, and upregulation of FTO could repress pyroptosis, inflammation, and oxidative stress in Dox-induced cardiomyocytes.

m^6A methylation is prominently elevated in Dox-induced cardiomyocytes, and FTO reduces m^6A-RNA methylation

A prior study reported that FTO effectively demethylates m^6A and that m^6A levels in mRNA are affected by the activity of FTO (23). Therefore, we explored the changes in m^6A methylation during Dox-stimulated HF and whether increased m^6A methylation is associated with changes in FTO demethylase activity. Polyadenylated mRNA was extracted for dot blot analysis after Dox treatment of H9C2 cells, which showed a marked increase in overall m^6A methylation in cells after Dox treatment (*Figure 3A,3B*). Furthermore, m^6A methylation was appreciably reduced in H9C2 cells after overexpression of FTO (*Figure 3C,3D*). In the cardiomyocyte model of Dox-induced HF, m^6A methylation was upregulated, and FTO, as a demethylase, could reduce m^6A RNA methylation.

TLR4 is upregulated in Dox-induced cardiomyocytes, and TLR4 knockdown suppresses pyroptosis, inflammation, and oxidative stress in Dox-induced cardiomyocytes

To clarify the specific biological significance and mechanism of TLR4 in HF development, TLR4 expression was first examined in H9C2 cardiomyocytes. The data revealed a significant increase in TLR4 expression in H9C2 cells after Dox treatment (*Figure 4A*). SiRNA of TLR4 was used to evaluate the effect of TLR4 on the biological function of Dox-treated cardiomyocytes. TLR4 expression was noticeably reduced following si-TLR4 transfection (*Figure 4B*). Additionally, further results (*Figure 4C-4F*) manifested that TLR4 knockdown observably decreased apoptosis and the levels of LDH, inflammatory factors, and MDA while markedly increasing SOD levels in Dox-treated H9C2 cells. In addition, the expression of pyroptosis proteins was diminished in response to TLR4 knockdown (*Figure 4G*). Immunofluorescence staining demonstrated a reduction in NLRP3 inflammasome levels in Dox-treated H9C2 cells after TLR4 knockdown, as evidenced by markedly decreased fluorescence intensity of NLRP3 inflammasomes (*Figure 4H*).

In conclusion, TLR4 downregulation impeded pyroptosis, inflammation, and oxidative stress in Dox-induced cardiomyocytes.

FTO functions as an m^6A demethylase, regulating the m^6A modification of TLR4 and downregulatingTLR4

To explore the relationship between FTO and TLR4 in

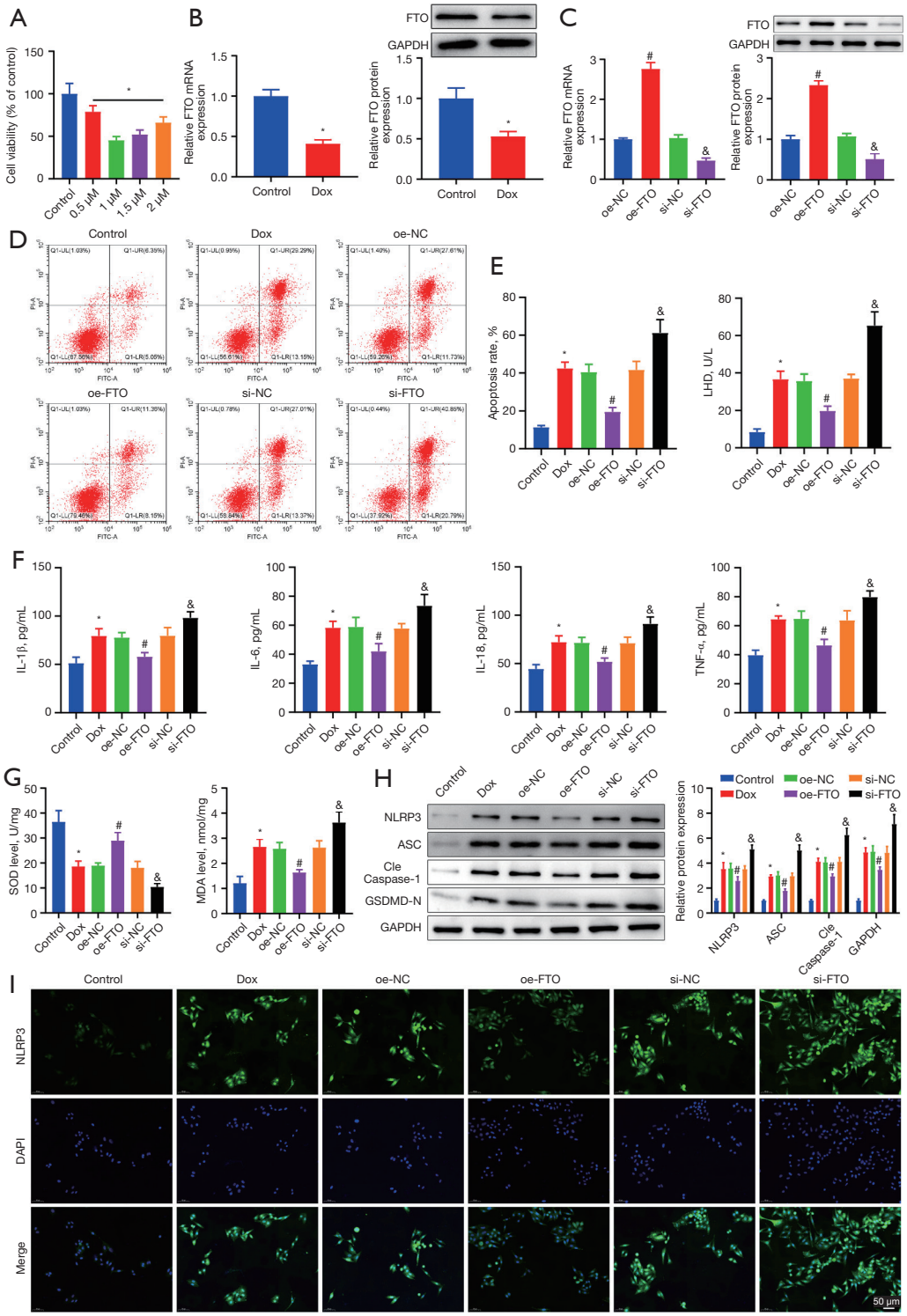

Figure 2 FTO is downregulated in Dox-treated cardiomyocytes, and FTO overexpression depresses pyroptosis, inflammation, and oxidative stress in Dox-induced cardiomyocytes. (A) Cardiomyocyte viability after treatment of different concentrations of Dox measured with CCK-8 assay. (B) RT-qPCR and western blotting to detect FTO expression in cardiomyocytes after Dox treatment. (C) RT-qPCR and western blotting to test FTO expression in cardiomyocytes after upregulation or knockdown of FTO. (D) Flow cytometry to examine apoptosis. (E) Detection of LDH expression. (F) Expression of inflammatory factors (IL-18, IL-1β, TNF-α, and IL-6) determined with

ELISA. (G) Expression of oxidative stress-related indicators (MDA and SOD). (H) Western blotting analysis of pyroptosis-related proteins (NLRP3, ASC, cleaved caspase-1, and GSDMD-N). (I) Immunofluorescence staining to measure the pyroptosis protein NLRP3. Data were expressed as mean ± standard deviation. Cell experiments were performed three times. Normally distributed data between two groups were compared with the unpaired *t*-test and among multiple groups were compared with one-way analysis of variance. Tukey's test was used for *post hoc* analysis. *, P<0.05 compared with the control group; #, P<0.05 compared with the oe-NC group; &, P<0.05 compared with the si-NC group. Dox, doxorubicin; FTO, fat mass and obesity-associated protein; GAPDH, glyceraldehyde-3-phosphate dehydrogenase; NC, negative control; FITC, fluorescein isothiocyanate; PI, propidium iodide; IL, interleukin; TNF-α, tumor necrosis factor alpha; MDA, malondialdehyde; SOD, superoxide dismutase; NLRP3, NOD-, LRR- and pyrin domain-containing protein 3; ASC, apoptosis-associated speck-like protein containing a CARD; GSDMD-N, gasdermin D N-terminal domain; DAPI, 4',6-diamidino-2-phenylindole; CCK-8, cell counting kit-8; RT-qPCR, reverse transcription quantitative polymerase chain reaction; LDH, lactic dehydrogenase; ELISA, enzyme-linked immunosorbent assay.

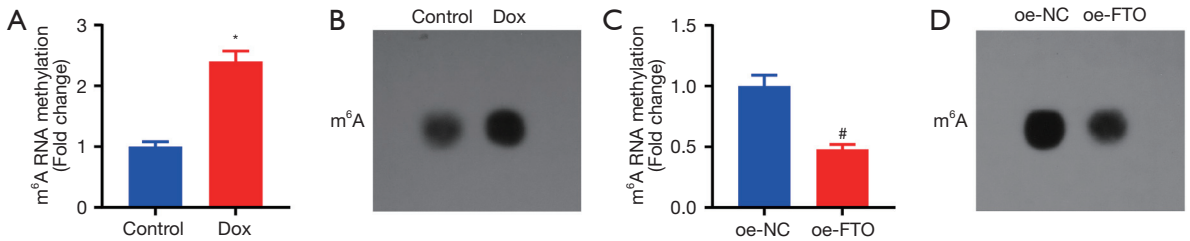

Figure 3 m^{6}A methylation is markedly increased in Dox-induced HF, and FTO lowers m^{6}A-RNA methylation. (A) Quantification of m^{6}A methylation levels in cardiomyocytes after Dox treatment. (B) RNA m^{6}A dot blot detection of methylation levels in cardiomyocytes. (C) Quantification of m^{6}A methylation levels in cardiomyocytes after overexpression of FTO. (D) RNA m^{6}A dot blot to measure methylation levels in cardiomyocytes. Data were expressed as mean ± standard deviation. Unpaired *t*-test was adopted for the comparison of two groups of data, with Tukey's test for *post hoc* test. *, P<0.05 compared with the control group; #, P<0.05 compared with the oe-NC group. Cell experiments were done three times. Dox, doxorubicin; m^{6}A, N6-methyladenosine; NC, negative control; FTO, fat mass and obesity-associated protein; HF, heart failure.

HF, FTO was overexpressed in H9C2 cells. RT-qPCR and western blotting results (*Figure 5A*) revealed that TLR4 expression was substantially reduced in response to oe-FTO transfection. Thereafter, we investigated the mechanism by which FTO regulated TLR4 expression in cardiomyocytes after Dox treatment. Since the aforementioned results illustrated that FTO could diminish m^{6}A RNA methylation, a series of experiments were carried out to ascertain whether TLR4 expression in cardiomyocytes was modified by FTO-mediated m^{6}A demethylation. Me-RIP assay revealed that Dox treatment significantly increased the m^{6}A modification level of TLR4 mRNA in H9C2 cells, but that this increase was suppressed by FTO overexpression in Dox-treated H9C2 cells (*Figure 5B*). In addition, the RIP assay was performed to clarify whether FTO could bind to TLR4 mRNA to eliminate m^{6}A modification, and the results (*Figure 5C*) presented that the m^{6}A modification of TLR4 mRNA was conspicuously reduced after overexpressing FTO. Subsequently, we investigated the mechanisms by which m^{6}A RNA modifications regulated TLR4 expression in HF. YTHDF1, YTHDF2, and YTHDF3 are the main known m^{6}A readers, among which YTHDF2 binds to mRNAs to accelerate their degradation, YTHDF1 enhances the translation efficiency by recruiting translation initiation factors into cells, and YTHDF3 promotes the synthesis of YTHDF1-cooperated proteins and regulates YTHDF2-mediated decay of m^{6}A-modified mRNA (19,24). The results mentioned above illustrated that m^{6}A RNA modification augmented TLR4 expression in H9C2 cells. We speculated that TLR4 transcripts might be a downstream target of YTHDF1. YTHDF1, YTHDF2, and YTHDF3 were siRNA-mediatedly downregulated in H9C2 cells to support this hypothesis. The data demonstrated that TLR4 expression was considerably decreased by YTHDF1 knockdown but was not signally changed after knockdown of YTHDF2 or YTHDF3 (*Figure 5D*). Meanwhile, the decay rate of TLR4 was prominently enhanced subsequent to knockdown of YTHDF1 but was lowered in response

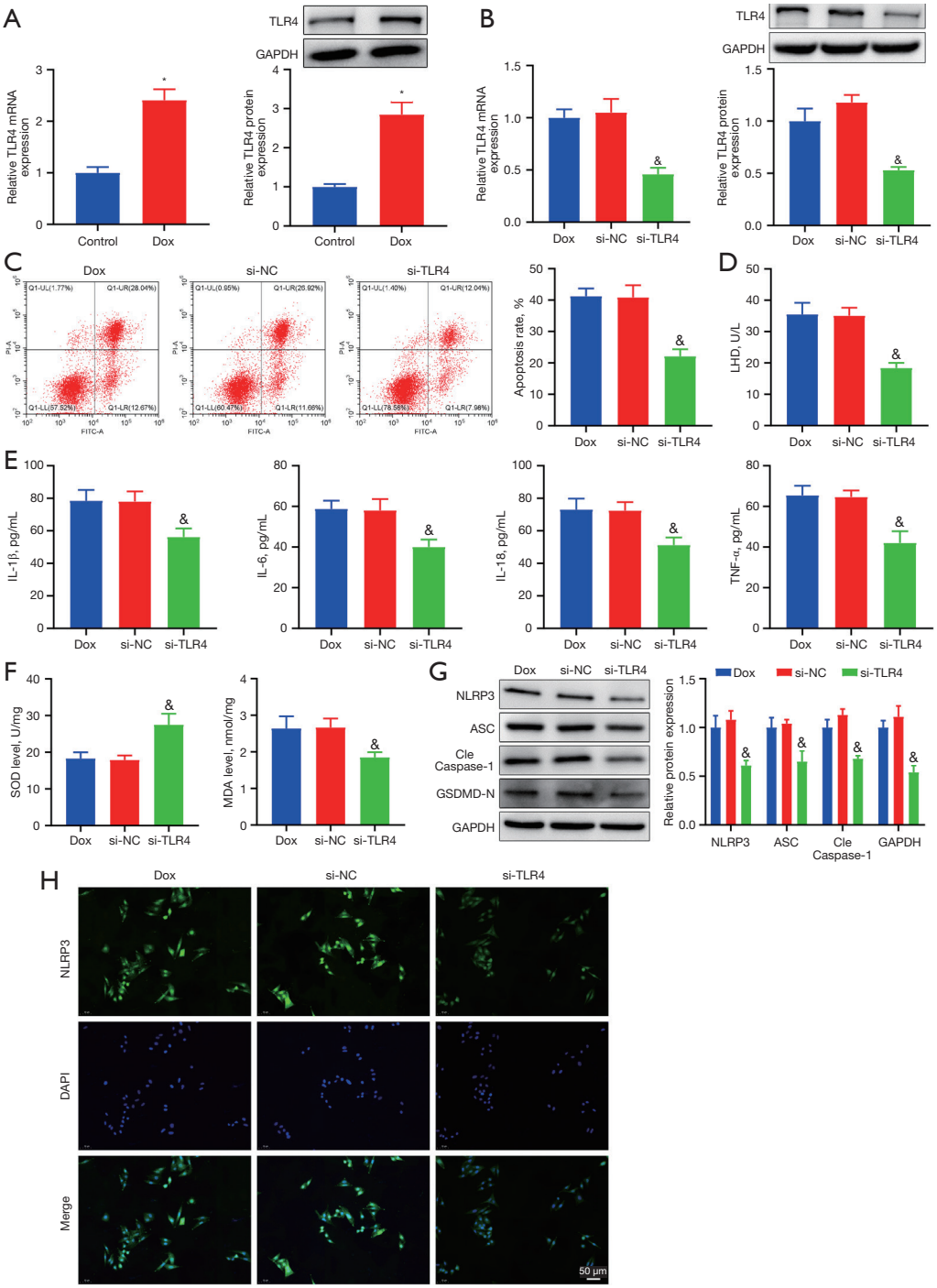

Figure 4 TLR4 expression is high in Dox-induced cardiomyocytes, and TLR4 downregulation inhibits pyroptosis, inflammation, and oxidative stress in Dox-induced cardiomyocytes. (A) RT-qPCR and western blotting to detect TLR4 expression in cardiomyocytes after Dox treatment. (B) RT-qPCR and western blotting to test TLR4 expression in cardiomyocytes after silencing TLR4. (C) Cardiomyocyte apoptosis measured with flow cytometry. (D) Determination of LDH expression. (E) Measurement of expression of inflammatory factors (IL-18, IL-1β, TNF-α, and IL-6). (F) Expression of oxidative stress-related indicators (MDA and SOD). (G) Western blotting of pyroptosis-related proteins (NLRP3, ASC, cleaved caspase-1, and GSDMD-N). (H) Immunofluorescence staining to assess NLRP3 expression in cardiomyocytes. Data were expressed as mean ± standard deviation. Normally distributed data were compared between two groups with the

unpaired *t*-test and among multiple groups with one-way analysis of variance. Tukey's test was used for *post hoc* analysis. *, P<0.05 compared with the control group; &, P<0.05 compared with the si-NC group. Cell experiments were done three times. Dox, doxorubicin; TLR4, toll-like receptor 4; GAPDH, glyceraldehyde-3-phosphate dehydrogenase; NC, negative control; FITC, fluorescein isothiocyanate; PI, propidium iodide; IL, interleukin; TNF-α, tumor necrosis factor alpha; SOD, superoxide dismutase; MDA, malondialdehyde; NLRP3, NOD-, LRR- and pyrin domain-containing protein 3; ASC, apoptosis-associated speck-like protein containing a CARD; GSDMD-N, gasdermin D N-terminal domain; DAPI, 4',6-diamidino-2-phenylindole; RT-qPCR, reverse transcription quantitative polymerase chain reaction; LDH, lactic dehydrogenase.

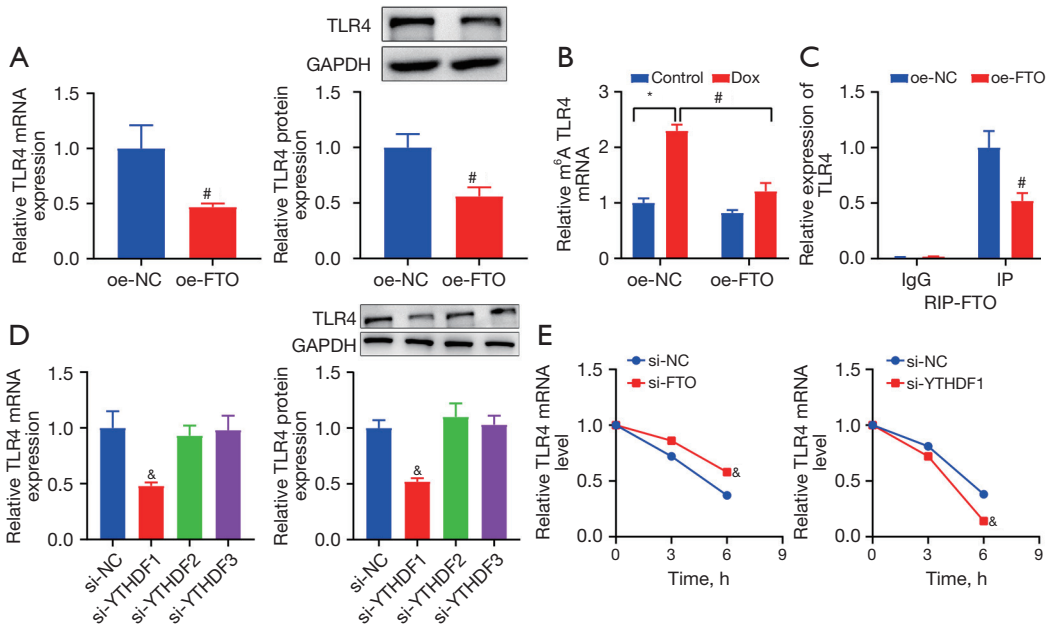

Figure 5 FTO decreases TLR4 expression by mediating the m^{6}A modification of TLR4. (A) TLR4 expression in cardiomyocytes after overexpression of FTO tested with RT-qPCR and western blotting. (B) The m^{6}A modification level of TLR4 mRNA examined with the Me-RIP assay. (C) RIP assay to determine TLR4 expression after overexpression of FTO. (D) TLR4 expression after knockdown of YTHDF1, YTHDF2, and YTHDF3 assessed with RT-qPCR and western blotting. (E) mRNA stability measurement by determining the TLR4 decay rate. Data were expressed as mean ± standard deviation. Normally distributed data were compared between two groups with the unpaired *t*-test and among multiple groups with one-way analysis of variance. Tukey's test was used for *post hoc* analysis. *, P<0.05 compared with the control group; #, P<0.05 compared with the oe-NC group; &, P<0.05 compared with the si-NC group. Cell experiments were done three times. NC, negative control; FTO, fat mass and obesity-associated protein; TLR4, toll-like receptor 4; GAPDH, glyceraldehyde-3-phosphate dehydrogenase; Dox, doxorubicin; RIP, RNA immunoprecipitation; m^{6}A, N6-methyladenosine; RT-qPCR, reverse transcription quantitative polymerase chain reaction; Me-RIP, methylated-RIP.

to FTO knockdown (*Figure 5E*). Overall, FTO, as an m^{6}A demethylase, reduced the m^{6}A modification of TLR4 mRNA through YTHDF1, which affects TLR4 expression.

FTO reduces pyroptosis, inflammation, and oxidative stress in Dox-induced cardiomyocytes via the TLR4/NF-κB pathway

A former study unveiled that TLR4 specifically recognized pathogen-associated molecules, which activated the phosphorylation, ubiquitination, and degradation of the NF-κB inhibitory protein IκB, inducing inflammatory factor release and inflammation (25). Therefore, to further study how FTO affects the biological behaviors of Dox-induced H9C2 cells via the TLR4/NF-κB pathway, Dox-treated H9C2 cells were subjected to co-transfection and were allocated into si-NC + si-NC, si-FTO + si-NC, and si-FTO + si-TLR4 groups. The transfection efficiency

was verified by measuring TLR4 expression. The results indicated that FTO knockdown resulted in an increase in TLR4 m^{6}A modification and elevated TLR4 expression, while TLR4 knockdown effectively lowered TLR4 expression in cardiomyocytes in the presence of FTO knockdown (*Figure 6A*). Next, p-NF-κB p65 and p-IκB-α expression was examined. In cardiomyocytes, TLR4 and p-NF-κB p65 expression was increased and p-IκB-α was substantially elevated after knockdown of FTO, which was neutralized by further TLR4 knockdown (*Figure 6B*). Meanwhile, the results of cell function assays displayed that TLR4 knockdown conspicuously diminished apoptotic rate and LDH levels in Dox-treated H9C2 cells in the presence of FTO knockdown (*Figure 6C,6D*). Additionally, the levels of inflammatory factors, oxidative stress, and pyroptosis proteins were greatly decreased (*Figure 6E-6G*). Immunofluorescence staining results (*Figure 6H*) revealed that TLR4 knockdown reversed the increased number of NLRP3 inflammasomes caused by FTO knockdown.

In conclusion, FTO affected p-NF-κB p65 and p-IκB-α expression via the TLR4/NF-κB pathway and thereby alleviated Dox-induced pyroptosis and inflammation in cardiomyocytes.

Discussion

Currently, Dox is vastly utilized for the treatment of various cancers, including leukemia, breast cancer, brain cancer, and thyroid cancer (26). Dox's strong affinity for cardiomyocytes predisposes to the cardiotoxicity of Dox, which leads to arrhythmias and chronic HF (27). Dox-induced HF is a severe disease given the well-known difficulties in its treatment (28). Therefore, the molecular mechanism of Dox-induced HF is warranted to be studied for the development of novel treatment. In our study, a cell model of Dox-induced HF was established in H9C2 cardiomyocytes to analyze the role and mechanism of FTO in Dox-induced HF. The findings unraveled that FTO mediated m^{6}A de-modification of TLR4 and regulated the binding activity of YTHDF1 to TLR4 mRNA to downregulate TLR4, thereby suppressing pyroptosis, inflammation, and oxidative stress in Dox-induced cardiomyocytes via the TLR4/NF-κB pathway.

FTO has been revealed to participate in numerous heart diseases. For instance, FTO exhibits reduced expression in mice with myocardial ischemia-reperfusion injury and hypoxia/reoxygenation (H/R)-induced cardiomyocytes (29). FTO deficiency has been linked to endotoxemia-caused myocardial inflammation and dysfunction in mice (30). Of note, FTO is upregulated in heart tissues of the HF mouse model established by intraperitoneal injection of Dox (31). Consistently, our data revealed that FTO was downregulated in serum of HF patients and Dox-induced cardiomyocytes. Moreover, a prior study elucidated the promoting role of FTO downregulation in H/R-treated cardiomyocyte apoptosis and oxidative stress (32). FTO overexpression protects protection from H/R-induced apoptosis and inflammation of cardiomyocytes (29). Meanwhile, FTO upregulation suppresses NLRP3 inflammasome-mediated pyroptosis in oxygen-glucose deprivation/reoxygenation-induced H9C2 cells (33). Of note, similar trends were observed in our study, which revealed that overexpressing FTO curbed pyroptosis, inflammation, and oxidative stress in Dox-treated cardiomyocytes.

m^{6}A orchestrates gene expression and therefore inhibits the activation of HF-related cell signaling pathways (34). Importantly, our data revealed a significant increase in m^{6}A methylation in Dox-treated cardiomyocytes. As an m^{6}A demethylase, FTO is required for the demethylation of m^{6}A and affects m^{6}A modification of mRNAs (35). A prior study unveiled that FTO overexpression contributed to the loss of m^{6}A in TLR4 mRNA in the hemorrhagic thalamus (13). Similarly, our research elucidated that FTO decreased m^{6}A-RNA methylation and the m^{6}A modification level of TLR4 mRNA in Dox-treated cardiomyocytes. YTHDF1 has been reported to increase the efficiency of mRNAs translation (24). In our study, YTHDF1 knockdown led to a reduction in TLR4 expression and an enhancement in the decay rate of TLR4. These results indicated that FTO as an m^{6}A demethylase declined the m^{6}A modification of TLR4 mRNA through YTHDF1 to downregulate TLR4. TLR4 is a crucial mediator of myocardial inflammation and plays a key role in the development of cardiovascular diseases (36). Tavakoli Dargani *et al.* noted TLR4 upregulation and NLRP3 inflammasome activation in Dox-treated H9C2 cells, which resulted in pyroptosis (15). Our study consistently demonstrated augmented TLR4 expression in serum of HF patients and in H9C2 cells subsequent to Dox treatment. Furthermore, TLR4 upregulation accelerated apoptosis, inflammation, and oxidative stress in H/R-treated cardiomyocytes, as evidenced by elevated reactive oxygen species (ROS), LDH, TNF-α, and IL-6 levels and decreased SOD levels (37). A prior study unraveled that TLR4 downregulation conferred protection against H/R-induced cardiomyocyte pyroptosis

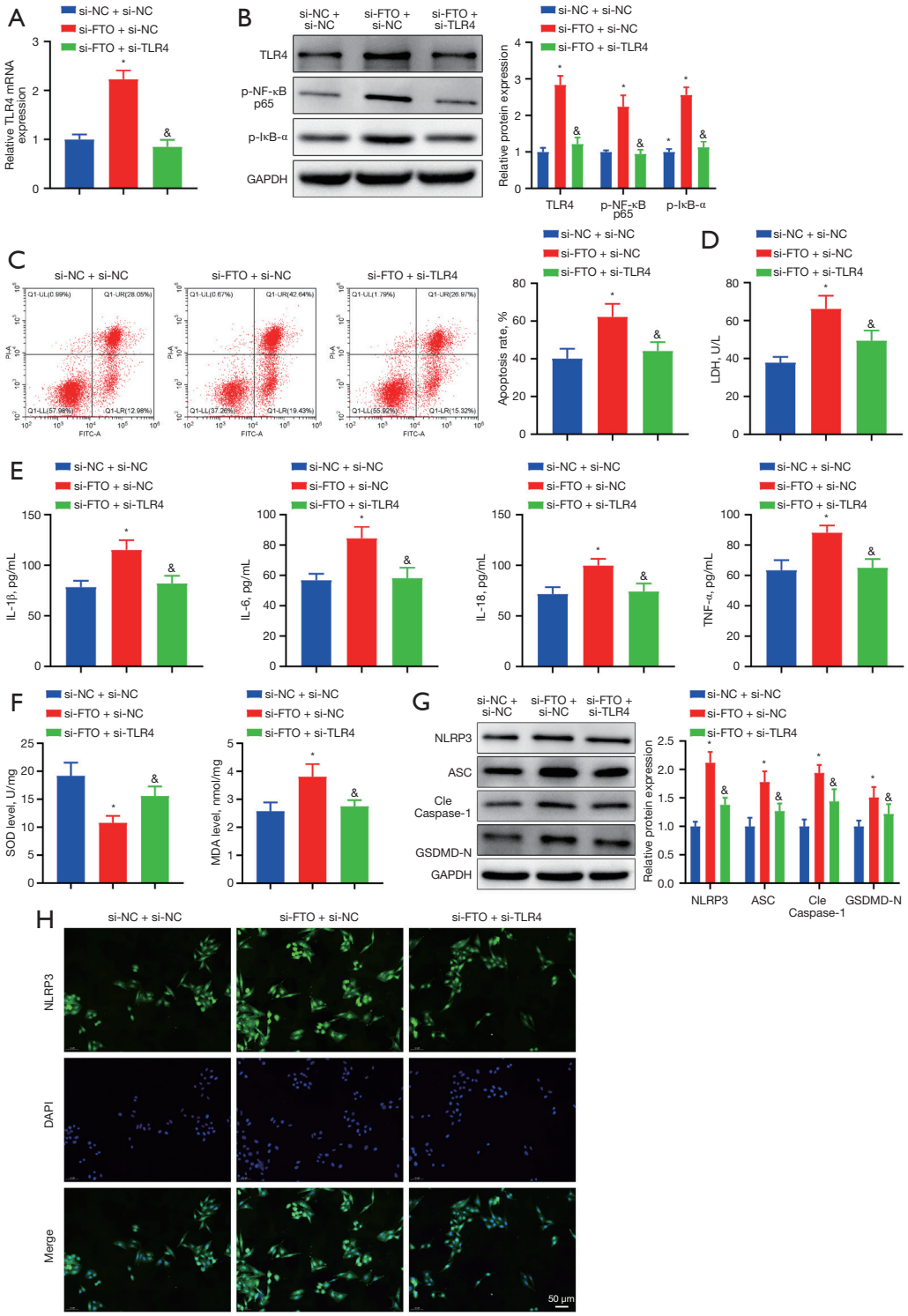

Figure 6 FTO represses pyroptosis and inflammation in Dox-induced cardiomyocytes through the TLR4/NF-κB pathway. (A) RT-qPCR to detect TLR4 expression in cardiomyocytes. (B) Western blotting to measure TLR4 expression and its downstream pathway proteins (p-NF-κB p65 and p-IκB-α). (C) Flow cytometry to test apoptosis. (D) LDH levels. (E) ELISA to examine the levels of inflammatory factors (IL-18, IL-1β, TNF-α, and IL-6). (F) Expression of oxidative stress-related indicators (MDA and SOD). (G) Western blotting analysis of pyroptosis-related proteins (NLRP3, ASC, cleaved caspase-1, and GSDMD-N). (H) Immunofluorescence staining to assess the expression of NLRP3.

Data were expressed as mean ± standard deviation. Data were compared among multiple groups with one-way analysis of variance. Tukey's test was used for *post hoc* analysis. *, P<0.05 compared with the si-NC + si-NC group; &, P<0.05 compared with the si-FTO + si-NC group. Cell experiments were done three times. NC, negative control; FTO, fat mass and obesity-associated protein; TLR4, toll-like receptor 4; GAPDH, glyceraldehyde-3-phosphate dehydrogenase; FITC, fluorescein isothiocyanate; PI, propidium iodide; LDH, lactic dehydrogenase; IL, interleukin; TNF-α, tumor necrosis factor alpha; SOD, superoxide dismutase; MDA, malondialdehyde; NLRP3, NOD-, LRR- and pyrin domain-containing protein 3; ASC, apoptosis-associated speck-like protein containing a CARD; GSDMD-N, gasdermin D N-terminal domain; DAPI, 4',6-diamidino-2-phenylindole; Dox, doxorubicin; RT-qPCR, reverse transcription quantitative polymerase chain reaction; ELISA, enzyme-linked immunosorbent assay.

by downregulating GSDMD, NLRP3, and caspase-1 (38). In our study, we found that TLR4 knockdown inhibited pyroptosis, inflammation, and oxidative stress in Dox-treated cardiomyocytes, thereby nullifying the effects of FTO knockdown.

NF-κB is the final effector molecule of the TLR4 pathway (39). The TLR4/NF-κB pathway has been demonstrated to participate in the regulation of isoproterenol-induced HF (40). Moreover, a prior study elaborated that the cardioprotective effect of baicalin against Dox-induced cardiotoxicity was achieved through the repression of the TLR4/NF-κB pathway (41). By inhibiting the TLR4/NF-κB pathway, sanguinarine reduces the inflammatory and apoptotic effects of lipopolysaccharide on cardiomyocytes (42). The activation of the TLR4/NF-κB pathway promotes pyroptosis in H/R-treated neonatal rat cardiomyocytes (43). A prior study unraveled that dexmedetomidine-induced TLR4 downregulation was accompanied by diminished p-NF-κB p65 and p-IκB-α levels in rats with lipopolysaccharide-induced acute lung injury (44). Concordantly, our data showed that p-NF-κB p65 and p-IκB-α expression was augmented by knockdown of FTO, which was abrogated by further TLR4 knockdown.

Conclusions

In conclusion, our results showed that FTO upregulation, via the TLR4/NF-κB pathway, protected Dox-induced cardiomyocytes from pyroptosis, inflammation, and oxidative stress. This study proposes FTO as a promising target for the prevention and treatment of Dox-induced HF. Our study does have some shortcomings, though. First off, more clinical studies are required before our experimental findings can be applied to clinical trials due to the small clinical sample size used in the study. Second, our experiments were conducted with only cells, and clinical and animal experiments are required in the future for further verification.

Acknowledgments

Funding: This work was supported by the National Natural Science Foundation of China (No. 82260078, to Shao Liang).

Footnote

Data Sharing Statement: Available at https://cdt.amegroups.com/article/view/10.21037/cdt-23-326/dss

Peer Review File: Available at https://cdt.amegroups.com/article/view/10.21037/cdt-23-326/prf

Conflicts of Interest: All authors have completed the ICMJE uniform disclosure form (available at https://cdt.amegroups.com/article/view/10.21037/cdt-23-326/coif). The authors have no conflicts of interest to declare.

Ethical Statement: The authors are accountable for all aspects of the work in ensuring that questions related to the accuracy or integrity of any part of the work are appropriately investigated and resolved. The study obtained the informed consent from all patients or their families. All patients or their families provided informed consent for the study. The study was approved by the Medical Ethics Committee of Jiangxi Provincial People's Hospital (No. 2022120210) and adhered to the Declaration of Helsinki (as revised in 2013).

References

1. Wu BB, Leung KT, Poon EN. Mitochondrial-Targeted Therapy for Doxorubicin-Induced Cardiotoxicity. Int J Mol Sci 2022;23:1912.
2. Christidi E, Brunham LR. Regulated cell death pathways in doxorubicin-induced cardiotoxicity. Cell Death Dis 2021;12:339.
3. Koleini N, Nickel BE, Edel AL, et al. Oxidized phospholipids in Doxorubicin-induced cardiotoxicity. Chem Biol Interact 2019;303:35-9.
4. Wallace KB, Sardão VA, Oliveira PJ. Mitochondrial Determinants of Doxorubicin-Induced Cardiomyopathy. Circ Res 2020;126:926-41.
5. Sheibani M, Azizi Y, Shayan M, et al. Doxorubicin-Induced Cardiotoxicity: An Overview on Pre-clinical Therapeutic Approaches. Cardiovasc Toxicol 2022;22:292-310.
6. Kitakata H, Endo J, Ikura H, et al. Therapeutic Targets for DOX-Induced Cardiomyopathy: Role of Apoptosis vs. Ferroptosis. Int J Mol Sci 2022;23:1414.
7. Tian C, Yang Y, Bai B, et al. Potential of exosomes as diagnostic biomarkers and therapeutic carriers for doxorubicin-induced cardiotoxicity. Int J Biol Sci 2021;17:1328-38.
8. Yu P, Zhang X, Liu N, et al. Pyroptosis: mechanisms and diseases. Signal Transduct Target Ther 2021;6:128.
9. Ping Z, Fangfang T, Yuliang Z, et al. Oxidative Stress and Pyroptosis in Doxorubicin-Induced Heart Failure and Atrial Fibrillation. Oxid Med Cell Longev 2023;2023:4938287.
10. He L, Li H, Wu A, et al. Functions of N6-methyladenosine and its role in cancer. Mol Cancer 2019;18:176.
11. Li Y, Su R, Deng X, et al. FTO in cancer: functions, molecular mechanisms, and therapeutic implications. Trends Cancer 2022;8:598-614.
12. Mathiyalagan P, Adamiak M, Mayourian J, et al. FTO-Dependent N(6)-Methyladenosine Regulates Cardiac Function During Remodeling and Repair. Circulation 2019;139:518-32.
13. Fu G, Du S, Huang T, et al. FTO (Fat-Mass and Obesity-Associated Protein) Participates in Hemorrhage-Induced Thalamic Pain by Stabilizing Toll-Like Receptor 4 Expression in Thalamic Neurons. Stroke 2021;52:2393-403.
14. Zhang Y, Liang X, Bao X, et al. Toll-like receptor 4 (TLR4) inhibitors: Current research and prospective. Eur J Med Chem 2022;235:114291.
15. Tavakoli Dargani Z, Singla DK. Embryonic stem cell-derived exosomes inhibit doxorubicin-induced TLR4-NLRP3-mediated cell death-pyroptosis. Am J Physiol Heart Circ Physiol 2019;317:H460-71.
16. Zhang Z, Peng J, Hu Y, et al. CTRP5 Attenuates Doxorubicin-Induced Cardiotoxicity Via Inhibiting TLR4/NLRP3 Signaling. Cardiovasc Drugs Ther 2023. [Epub ahead of print]. doi: 10.1007/s10557-023-07464-x.
17. Yu C, Wang D, Yang Z, et al. Pharmacological Effects of Polyphenol Phytochemicals on the Intestinal Inflammation via Targeting TLR4/NF-κB Signaling Pathway. Int J Mol Sci 2022;23:6939.
18. Feng P, Yang Y, Liu N, et al. Baicalin regulates TLR4/IκBα/NFκB signaling pathway to alleviate inflammation in Doxorubicin related cardiotoxicity. Biochem Biophys Res Commun 2022;637:1-8.
19. Jiang X, Liu B, Nie Z, et al. The role of m6A modification in the biological functions and diseases. Signal Transduct Target Ther 2021;6:74.
20. Du J, Liao W, Liu W, et al. N(6)-Adenosine Methylation of Socs1 mRNA Is Required to Sustain the Negative Feedback Control of Macrophage Activation. Dev Cell 2020;55:737-753.e7.
21. Qing Y, Dong L, Gao L, et al. R-2-hydroxyglutarate attenuates aerobic glycolysis in leukemia by targeting the FTO/m(6)A/PFKP/LDHB axis. Mol Cell 2021;81:922-939.e9.
22. Song H, Feng X, Zhang H, et al. METTL3 and ALKBH5 oppositely regulate m(6)A modification of TFEB mRNA, which dictates the fate of hypoxia/reoxygenation-treated cardiomyocytes. Autophagy 2019;15:1419-37.
23. Jia G, Fu Y, Zhao X, et al. N6-methyladenosine in nuclear RNA is a major substrate of the obesity-associated FTO. Nat Chem Biol 2011;7:885-7.
24. Zhang B, Jiang H, Dong Z, et al. The critical roles of m6A modification in metabolic abnormality and cardiovascular diseases. Genes Dis 2020;8:746-58.
25. Luo QJ, Sun MX, Guo YW, et al. Sodium butyrate protects against lipopolysaccharide-induced liver injury partially via the GPR43/ β-arrestin-2/NF-κB network. Gastroenterol Rep (Oxf) 2020;9:154-65.
26. Jones IC, Dass CR. Doxorubicin-induced cardiotoxicity: causative factors and possible interventions. J Pharm Pharmacol 2022;74:1677-88.
27. Yun W, Qian L, Yuan R, et al. Periplocymarin Alleviates Doxorubicin-Induced Heart Failure and Excessive

Accumulation of Ceramides. Front Cardiovasc Med 2021;8:732554.
28. Christiansen S. Clinical management of doxorubicin-induced heart failure. J Cardiovasc Surg (Torino) 2011;52:133-8.
29. Ke WL, Huang ZW, Peng CL, et al. m(6)A demethylase FTO regulates the apoptosis and inflammation of cardiomyocytes via YAP1 in ischemia-reperfusion injury. Bioengineered 2022;13:5443-52.
30. Dubey PK, Patil M, Singh S, et al. Increased m6A-RNA methylation and FTO suppression is associated with myocardial inflammation and dysfunction during endotoxemia in mice. Mol Cell Biochem 2022;477:129-41.
31. Shen W, Li H, Su H, et al. FTO overexpression inhibits apoptosis of hypoxia/reoxygenation-treated myocardial cells by regulating m6A modification of Mhrt. Mol Cell Biochem 2021;476:2171-9.
32. Wen C, Lan M, Tan X, et al. GSK3β Exacerbates Myocardial Ischemia/Reperfusion Injury by Inhibiting Myc. Oxid Med Cell Longev 2022;2022:2588891.
33. Sun F, An C, Liu C, et al. FTO represses NLRP3-mediated pyroptosis and alleviates myocardial ischemia-reperfusion injury via inhibiting CBL-mediated ubiquitination and degradation of β-catenin. FASEB J 2023;37:e22964.
34. Liu S, Wang T, Cheng Z, et al. N6-methyladenosine (m6A) RNA modification in the pathophysiology of heart failure: a narrative review. Cardiovasc Diagn Ther 2022;12:908-25.
35. Yang Z, Yu GL, Zhu X, et al. Critical roles of FTO-mediated mRNA m6A demethylation in regulating adipogenesis and lipid metabolism: Implications in lipid metabolic disorders. Genes Dis 2022;9:51-61.
36. Xu Y, Chen S, Cao Y, et al. Discovery of novel small molecule TLR4 inhibitors as potent anti-inflammatory agents. Eur J Med Chem 2018;154:253-66.
37. Zhang S, Wang Y, Wang P, et al. miR-708 affords protective efficacy in anoxia/reoxygenation-stimulated cardiomyocytes by blocking the TLR4 signaling via targeting HMGB1. Mol Cell Probes 2020;54:101653.
38. Wei L, Zhao D. M2 macrophage-derived exosomal miR-145-5p protects against the hypoxia/reoxygenation-induced pyroptosis of cardiomyocytes by inhibiting TLR4 expression. Ann Transl Med 2022;10:1376.
39. Luo H, Guo P, Zhou Q. Role of TLR4/NF-κB in damage to intestinal mucosa barrier function and bacterial translocation in rats exposed to hypoxia. PLoS One 2012;7:e46291.
40. Sun H, Bai J, Sun Y, et al. Oxymatrine attenuated isoproterenol-induced heart failure via the TLR4/NF-κB and MAPK pathways in vivo and in vitro. Eur J Pharmacol 2023;941:175500.
41. El-Ela SRA, Zaghloul RA, Eissa LA. Promising cardioprotective effect of baicalin in doxorubicin-induced cardiotoxicity through targeting toll-like receptor 4/nuclear factor-κB and Wnt/β-catenin pathways. Nutrition 2022;102:111732.
42. Meng YY, Liu Y, Hu ZF, et al. Sanguinarine Attenuates Lipopolysaccharide-induced Inflammation and Apoptosis by Inhibiting the TLR4/NF-κB Pathway in H9c2 Cardiomyocytes. Curr Med Sci 2018;38:204-11.
43. Dai Y, Wang S, Chang S, et al. M2 macrophage-derived exosomes carry microRNA-148a to alleviate myocardial ischemia/reperfusion injury via inhibiting TXNIP and the TLR4/NF-κB/NLRP3 inflammasome signaling pathway. J Mol Cell Cardiol 2020;142:65-79.
44. Meng L, Li L, Lu S, et al. The protective effect of dexmedetomidine on LPS-induced acute lung injury through the HMGB1-mediated TLR4/NF-κB and PI3K/Akt/mTOR pathways. Mol Immunol 2018;94:7-17.

Cite this article as: Tu W, Huang X, Liu S, Zhan Y, Cai X, Shao L. The m^{6}A demethylase fat mass and obesity-associated protein mitigates pyroptosis and inflammation in doxorubicin-induced heart failure via the toll-like receptor 4/NF-κB pathway. Cardiovasc Diagn Ther 2024;14(1):158-173. doi: 10.21037/cdt-23-326

